NANO LETTERS

Letter

Nanoimprint Lithography for Nanophotonics in Silicon

Christiaan M. Bruinink, Matteo Burresi, Meint J. de Boer, Frans B. Segerink, Henri V. Jansen, E. Berenschot, David N. Reinhoudt, Jurriaan Huskens, and L. Kuipers

Nano Lett., **2008**, 8 (9), 2872-2877 • DOI: 10.1021/nl801615c • Publication Date (Web): 12 August 2008

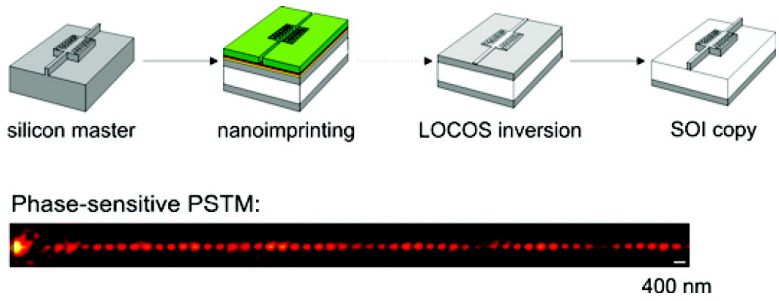

More About This Article

Additional resources and features associated with this article are available within the HTML version:

- Supporting Information
- Access to high resolution figures
- Links to articles and content related to this article
- Copyright permission to reproduce figures and/or text from this article

View the Full Text HTML

Nano Letters is published by the American Chemical Society. 1155 Sixteenth Street N.W., Washington, DC 20036

NANO LETTERS

2008
Vol. 8, No. 9
2872-2877

Nanoimprint Lithography for Nanophotonics in Silicon

Christiaan M. Bruinink,[†] Matteo Burresi,[‡] Meint J. de Boer,[§] Frans B. Segerink,[||] Henri V. Jansen,[§] E. Berenschot,[§] David N. Reinhoudt,[†] Jurriaan Huskens,[*,†] and L. Kuipers[*,‡]

Molecular Nanofabrication Group, MESA+ Institute for Nanotechnology, University of Twente, P.O. Box 217, NL-7500 AE Enschede, The Netherlands, Transducer Science & Technology, MESA+ Institute for Nanotechnology, University of Twente, P.O. Box 217, NL-7500 AE Enschede, The Netherlands, Optical Sciences, MESA+ Institute for Nanotechnology, University of Twente, P.O. Box 217, NL-7500 AE Enschede, The Netherlands, and Center for Nanophotonics, FOM Institute for Atomic and Molecular Physics (AMOLF), Kruislaan 407, NL-1098 SJ Amsterdam, The Netherlands

Received June 5, 2008; Revised Manuscript Received July 14, 2008

ABSTRACT

A novel inverse imprinting procedure for nanolithography is presented which offers a transfer accuracy and feature definition that is comparable to state-of-the-art nanofabrication techniques. We illustrate the fabrication quality of a demanding nanophotonic structure: a photonic crystal waveguide. Local examination using photon scanning tunneling microscopy (PSTM) shows that the resulting nanophotonic structures have excellent guiding properties at wavelengths in the telecommunications range, which indicates a high quality of the local structure and the overall periodicity.

Photonic crystals (PhCs)[1,2] have been a fascinating and active field of research in the past decade owing to the ability of these artificial nanostructures to influence the generation and propagation of light.[3,4] In particular, due to the periodic dielectric structure, PhCs may prohibit the propagation of photons of a certain range of frequencies (known as the photonic bandgap). The flexibility to tune the optical properties by changing the local geometry in PCs results in novel types of filters, couplers, lasers,[5] waveguides,[6] etc. For example, by incorporating structural line defects within a (perfect) two-dimensional PhC in thin dielectric slabs one can fabricate low-loss photonic crystal waveguides (PhCWGs). The fabrication of these 2D PhCWGs on oxide claddings of commercially available high-quality silicon-on-insulator (SOI) wafers has become the most dominant in scientific research as it allows the direct application of the mature tools of silicon nanofabrication technology, e.g., direct e-beam lithography (EBL)[7] and deep-UV (DUV) lithography,[8] for high-resolution pattern generation in combination with any deposition and/or dry etching tool to transfer the final devices into SOI.[9]

So far, less attention has been given to the low-cost fabrication of 2D PhCWGs. Generally, photonic-crystal-based nanophotonic devices pose very stringent requirements on the quality of the nanofabrication technique. Not only does the definition of the local features, typically nanoholes in a background of high-index material, need to be perfect, but also the period of the crystal lattice has to be constant throughout the entire device. While local imperfections will lead to scattering losses, long-range imperfections, such as a nonconstant period, will lead to undesirable variations in the propagation constant and potentially in reflections and out-of-plane losses. From the set of emerging nanofabrication techniques, nanoimprint lithography (NIL)[10] has the highest potential for becoming the next-generation high-resolution lithography because of its high transfer accuracy, cost effectiveness, and high throughput even for structures that require sub-10-nm resolution. The research and development of NIL as a tool in the fabrication process of 2D PhCWGs is only very recent. After the first successful demonstration of low-cost replication of PhCWGs in polymers by so-called thermal NIL[11] in 2005, two groups have pioneered the replication of 2D PhCWGs on SOI by exploiting NIL.[12,13]

* Corresponding authors. (J.H.) E-mail: j.huskens@utwente.nl. Phone: +31-53-489-2980. Fax: +31-53-489-4645. (L.K.) E-mail: l.kuipers@amolf.nl. Phone. +31-20-608-1234. Fax: +31-20-668-4106.

[†] Molecular Nanofabrication group, MESA+ Institute for Nanotechnology.

[‡] Center for Nanophotonics, FOM Institute for Atomic and Molecular Physics (AMOLF).

[§] Transducer Science & Technology, MESA+ Institute for Nanotechnology.

[||] Optical Sciences, MESA+ Institute for Nanotechnology.

10.1021/nl801615c CCC: $40.75
Published on Web 08/12/2008

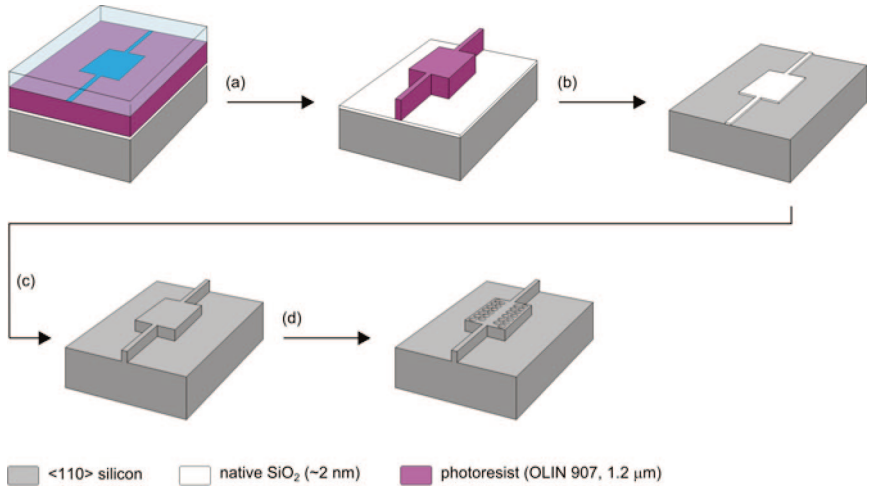

Figure 1. Schematic representation of the lithographic procedure for the fabrication of thermal NIL molds. (a) Exposure of positive photosensitive resist through a mask containing the outline structures of the waveguides followed by a development step. (b) Wet etching of the native SiO_2 and removal of the photoresist patterns. (c) Anisotropic wet etching of <110> silicon exploiting the native SiO_2 as the etch mask. (d) Local FIB milling of the photonic elements.

By the fabrication of a photonic crystal waveguide, we will demonstrate here that our novel inverse imprinting procedure for nanolithography has an exceptional pattern transfer accuracy in terms of feature dimension loss and feature definition. The novelty with respect to the current multilayer resist systems[14,15] lies in the fact that this procedure implements, for the first time, local oxidation of silicon (LOCOS),[16] a microfabrication isolation technique for VLSI, in the inversion of NIL resist patterns into thermal silicon oxide (SiO_2). By means of setting up design rules with respect to the thickness of the pattern transfer layers, etch selectivities, and silicon oxidation time, we will demonstrate a pattern inversion with close-to-zero feature dimension loss. The quality of the waveguide is interrogated with a phase-sensitive near-field optical microscope. With this local technique we demonstrate the absence of clear localized high-intensity spots, which would have been indicative of significant local imperfection of the structure. By exploiting the phase sensitivity we prove that the dispersion of the light is constant throughout the structure, which shows a high accuracy in the period. In addition, we report the first loss measurements on PhCWGs fabricated by nanoimprint procedures and find encouragingly low losses.

The fabrication process starts with the fast prototyping of silicon molds containing 2D PhCWGs combining conventional optical lithography to define the micron-scale ridge waveguides on larger areas and focused ion beam (FIB) milling to locally introduce the photonic crystal structure into the corresponding section within the waveguide outline structures (Figure 1).

The most important ingredient for consideration in this fabrication procedure is the type of etch technique to transfer photoresist waveguide patterns into silicon as any surface roughness could potentially cause detrimental losses for light propagation through the resulting 2D PhCWGs.[17] One potential silicon etching technique that is known to result in ultralow surface roughness is the anisotropic wet etching of silicon using basic aqueous solutions like commercially available resist developer OPD 4262,[18] which can achieve a surface finish with a surface roughness, $R_a < 0.5$ nm, for <110> p-type silicon.[19] As a result of the high etch selectivity, native SiO_2 was found to be a suitable etch mask in the present procedure to anisotropically etch the resist patterns into the top silicon layer of the SOI substrate in OPD 4262. Finally, the photonic crystal structures were written into the resulting silicon waveguide outline structures of the silicon mold by FIB milling.

The structural design of the photonic elements (hole diameter $d = 214$ nm, periodicity $a = 390$ nm) was based on the work of Notomi and co-workers, which illustrated excellent single-mode transmission efficiencies for the transverse-electric (TE) polarization with narrow, W0.7 line-defect PhCWGs on SOI.[7,20,21] The final silicon mold, consisting of narrow (W0.7) line-defect 2D PhCWGs with a total length of about 22 μm (or 56a) in between 2 μm-wide ridge waveguides, is shown in Figure 2a.

At the stage of FIB milling, special care was taken to match the 2D PhCWG configuration to the waveguide outline structures. Besides the accurate positioning and milling of the photonic elements within the silicon waveguide outline structures, the close-up of Figure 2a illustrates the excellent circular definition of the photonic elements. Feature dimension analysis of the silicon mold illustrates that the feature diameter was about 14 nm larger than the design geometry of the PhCWG.[23] The periodicity conforms excellently to the design setting.

The inverse imprinting procedure to replicate the 2D PhCWGs into SOI is shown in Figure 3. This procedure builds on the local oxidation of silicon (LOCOS) procedure[16] in order to invert polymer imprint patterns of 2D PhCWGs. Substrate preparation was done in order to allow for accurate pattern transfer: (i) deposition of two ultrathin transfer layers by low-pressure chemical vapor deposition (LPCVD) (in the order SOI substrate, silicon nitride (Si_3N_4, 14 nm), LPCVD−silicon oxide (SiO_2, 12 nm)) and (ii) high-temperature annealing of the substrate under dry nitrogen to facilitate

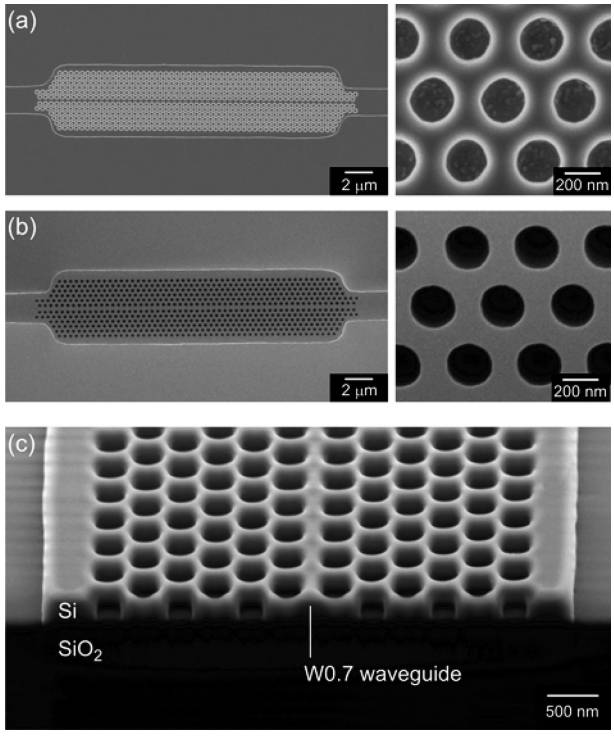

Figure 2. SEM images at different stages of the fabrication and replication procedure: (a) NIL mold ($d = 228 \pm 4$ nm, $a = 396 \pm 6$ nm), (b) final 2D PhCWG on SOI ($d = 228 \pm 2$ nm, $a = 392 \pm 4$ nm),[22] and (c) cross-section of the 2D PhCWG on SOI.

accurate pattern transfer during the wet etching of these two transfer layers in terms of resolution, etch rates, and etch selectivity.

For imprinting of the 2D PhCWG structures into polymers, the conditions for imprinting were set to a temperature ~80 °C above the glass-transition temperature and a pressure of 50 bar during an imprint time of 2 min. This procedure could be repeated for several tens of imprints without any observable deterioration of the silicon mold. Patterning of the first transfer layer (LPCVD−SiO_2) in 1% HF using thin (~100 nm) polymer etch masks by thermal NIL essentially requires HF-impermeable polymers (or high LPCVD-SiO_2 etch rates). High molecular weight PMMA ($M_w = 996$ kDa) was found to resist 1% HF for at least 2 min and was therefore the polymer of choice in the NIL replication step. The intrinsic thin residual polymer layer was removed by anisotropic O_2 RIE to preserve the lateral dimensions of the PMMA features and, as a result, the accuracy of the present replication process. The O_2 plasma had no significant effect on the surface roughness, as witnessed by AFM and as was shown before.[24] For process considerations, the only important side effect of the O_2 plasma treatment is the increase in the hydrophilicity of the PMMA layer. This effect could facilitate etching of the first pattern transfer layer, i.e., LPCVD−SiO_2, in the aqueous etching solution using PMMA as the etch mask. After subsequent transfer of the PMMA imprint patterns into LPCVD−SiO_2 (Figure 3b) and Si_3N_4 (Figure 3c) by etching in 1% HF and by 85% H_3PO_4 at 180 °C, respectively, the SOI substrates were put in a dry oxidation furnace to perform the final pattern inversion by LOCOS using the ultrathin Si_3N_4 patterns as oxidation masks (Figure 3d). Feature dimension analysis of the different stages of the replication process illustrates that the lateral encroachment of thermal SiO_2 under the Si_3N_4 mask during LOCOS[16] was effectively capable of canceling the increase in feature dimensions during the preceding wet-etch steps of the transfer layers.

The last step in the replication of the 2D PhCWGs was the cryogenic anisotropic etching into SOI (Figure 3e). At a silicon etch rate of ~600 nm·min^{-1} and an etch selectivity of silicon to thermal SiO_2 of ~50, the current anisotropic etch recipe allows for accurate etching with sufficient latitude to intercept the effect of RIE lag. RIE lag is the aspect ratio-dependent etching that occurs during the simultaneous etching of different features sizes due to ion depletion and redeposition.[25] The magnitude of RIE lag in the etching of the present PhCWG, i.e., the 300 μm interspaces between the waveguides and the ~230 nm holes of the photonic element, was ~5% according to cross-section examination of a substrate by high-resolution SEM. Some overetching (on the order of 20% with respect to the theoretical etching time) was done to ensure complete transfer into the top silicon layer, with the SiO_2 layer acting as an etch stop. The final 2D PhCWG on SOI is shown in Figure 2b after stripping the thermal SiO_2 etch mask in 1% HF. Feature dimension analysis by SEM illustrates that overall pattern transfer accuracy the 2D PhCWGs on SOI by the inverse imprinting procedure is competitive in terms of feature lateral dimensions (within 4 nm in comparison to the dimensions of the silicon mold) and feature definition to the accuracy of state-of-the-art nanolithographic techniques, e.g., direct e-beam lithography and focused ion-beam lithography. Additionally, the current critical feature dimension of NIL of 5 nm[26] implies that the present inversion procedure could also become competitive in terms of pattern resolution capability. SEM cross-section analysis in Figure 2c illustrates a high-quality anisotropic etch profile.

To investigate the optical quality of the present 2D PhCWG we exploited photon scanning tunneling microscopy (PSTM),[27] which has the capacity to investigate the propagation of light inside the line defect of 2D PhCWGs with subwavelength resolution.[28] Recently, slow light propagation in 2D PhCWGs has been shown by exploiting the scanning near-field optical microscope.[29] The visualization of the optical propagation allows a direct "eye-balling" of scattering at imperfections. The losses were measured directly on one structure, without requiring multiple structures for a (virtual) cut-back measurement.[30] Here, we have taken advantage of the phase-sensitive PSTM to elucidate the dispersion properties of 2D PhCWGs by measuring the local amplitude and phase of the light. In this way, the accuracy in the periodicity of the crystal becomes accessible.

Figure 4 illustrates the outcome of a typical PSTM measurement on our 2D PhCWGs. In the topographical image (Figure 4a), which was acquired by the height feedback mechanism during measurement of the optical information by scanning the near-field probe across the sample structure, the triangular lattice of the air holes (a) as well as the narrow line defect of the 2D PhCWG ($W = 472$

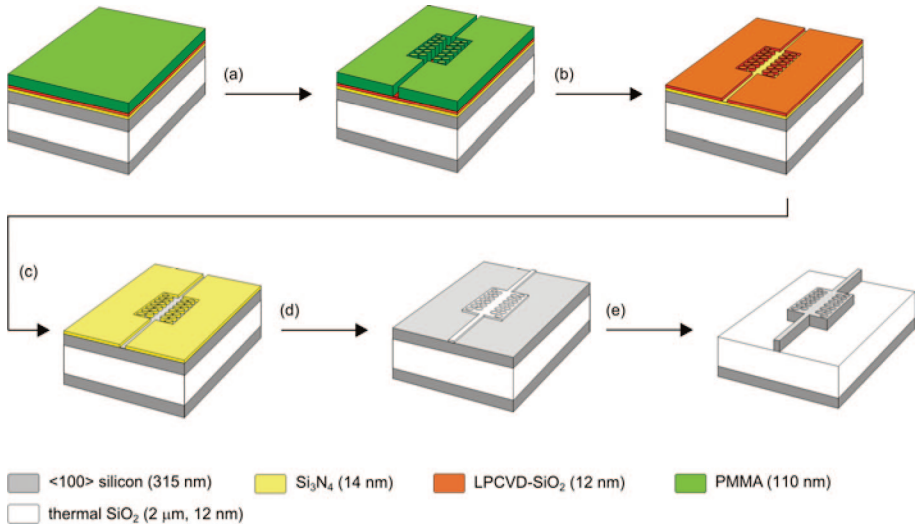

Figure 3. Schematic representation of the lithographic procedure for the replication of the 2D PhCWGs on SOI substrates: (a) thermal NIL in PMMA (and removal of the residual layer by O_2 plasma); (b) wet etching of LPCVD−SiO_2 using the PMMA imprint as the etch mask and removal of PMMA; (c) wet etching of Si_3N_4 and removal of the LPCVD SiO_2 etch mask; (d) dry oxidation of silicon and removal of the Si_3N_4 oxidation; (e) cryogenic etching of the final 2D PhCWGs in the top silicon layer of the SOI substrate.

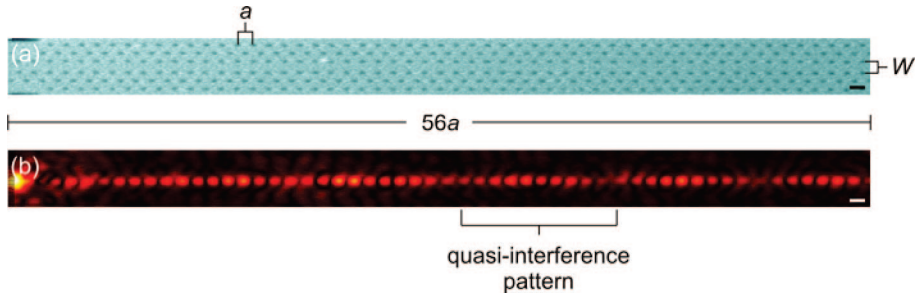

Figure 4. Phase-sensitive PSTM measurement of the 2D PhCWG under investigation: (a) measured topographical image of the 2D PhCWG revealing the triangular arrangement of the air holes; (b) measured optical field distribution (amplitude) image of the propagating light (λ_o = 1575 nm). The light is incident into the 2D PhCWG from the left. The scale bar in the images denotes a lateral dimension of 400 nm.

nm) are clearly resolved. The optical amplitude image (Figure 4b) reveals that the propagating light is highly confined to the line defect in the 2D PhC; the amplitude outside the defect is more than 1 order of magnitude smaller at a distance equal to a single lattice unit. Apart from the high amplitude at the transition between the access waveguide and the 2D PhCWG, no high amplitude spikes are present, which would have revealed scattering at local imperfections. On closer examination, a periodicity is apparent in the amplitude signal which is equal to the lattice constant of the 2D PhCWG. This periodicity was found to remain constant irrespective of the excitation frequency of the light.[31] This is a clear manifestation of the fact that the light propagating in the periodic waveguide is governed by Bloch's theorem,[32] which is indicative of a high definition of the periodicity of the 2D PhCWG. Another striking feature, albeit faint, in the amplitude image is the presence of a larger periodic modulation along the waveguide with a periodicity of about 10a (or ∼4 μm) as indicated in Figure 4b. This feature can be attributed to the quasi-interference between TE-like and TM-like modes.[32]

Fourier transformation enables us to determine the spatial frequencies of the propagating light: the wavevectors. By repeating this procedure as a function of the optical frequency through tuning of the laser, the photonic band diagram of the 2D PhCWG was measured in the excitation wavelength range from 1496 nm (ω = 0.262) up to 1592 nm (ω = 0.246).[33] Several separate photonic modes are apparent in Figure 5: the fundamental TE-like mode and the TM-like modes, indicated by the white and black arrows, respectively, propagating in forward direction. That these modes are found at spatial frequencies k and $k - 2\pi/a$ is direct proof that the light propagating inside the 2D PhCWG experiences a periodic modulation of the dielectric constant. The TE-like mode bends toward the edge of the Brillouin zone ($k = \pi$/a), near ω = 0.245. Apart from a slight shift of $\Delta\omega$ = 0.005, the measured photonic band structure is in qualitative agreement with the calculations of Notomi.[20] A strong dispersion is apparent at the Brillouin zone edge leading to slow light between λ_o 1575 nm (ω = 0.249) and 1590 nm (ω = 0.247). The measured photonic band structure reflects only a minimal amount of light propagating in the backward direction. This observation again attests to the high quality of the present nanophotonic device.

Phase-sensitive PSTM also allows us to quantify the propagation losses of the light inside a single line defect.

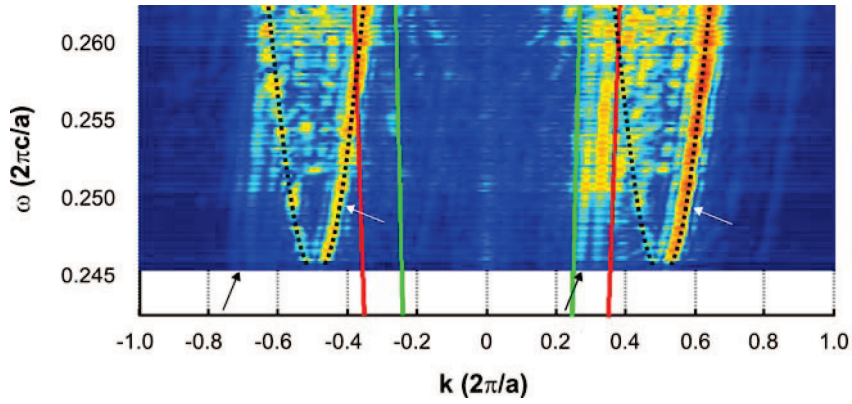

Figure 5. Experimentally determined photonic band diagram of the 2D PhCWG. The arrows in the band diagram indicate the dispersion curves of different modes of the waveguide: the dispersion curves indicated with the white arrows are both part of the TE-like mode and the curves indicated by the black arrows both belong to the TM-like mode. The green and red lines are the light lines in vacuum and in SiO_2, respectively. The black dotted lines serve as a guide to the eye for the TE mode.

By selecting specific modes in reciprocal space, one can determine the losses of only the mode of interest, i.e., the TE mode. By measuring the decay of the amplitude directly as a function of position, the need for investigating other reference structures is not necessary and the measurement is insensitive to the potential influence of coupling losses (the so-called insertion losses) at the interface of the access ridge waveguide and the 2D PhCWG. Below the cutoff frequency, i.e., when no modes are allowed to propagate in the waveguide, the penetration length of the light inside the line defect of the 2D PhCWG was found to be $\sim 2\ \mu$m. For frequencies above the cutoff frequency and below the SiO_2 light line, the forward propagating mode was selected in reciprocal space[34] and, from its decay as a function of position, losses down to 36 dB·mm^{-1} were found close to the cutoff frequency.[35] By selecting the backward propagating mode, it was observed that the loss induced by reflection (due to a combination of small defects inside the photonic structure and insertion loss at the end of the photonic crystal waveguide and the start of the exiting ridge waveguide) is only 4%. The main source of losses is due to out-of-plane scattering. While these losses are higher than the propagation losses obtained by Notomi,[20] these results are highly encouraging, first, because our measurements represent the first loss measurements on high-index photonic crystal waveguides fabricated with NIL, and second, because it is anticipated that tuning the silicon slab thickness from the $0.8a$ in the present 2D PhCWGs to the optimal slab thickness of $0.4-0.5a$[36] and transforming into an air-bridge type waveguide should significantly reduce the propagation losses.

In conclusion, the inverse imprinting procedure by combining thermal NIL, LOCOS, and cryogenic RIE is very accurate in terms of the overall pattern transfer accuracy (deviation in lateral dimension of <4 nm) and feature definition of the final 2D PhCWG on SOI. This process shows the highest pattern transfer accuracy to date in the replication of 2D PhCWGs into SOI by NIL and is therefore a viable alternative nanofabrication technique for nanophotonics. The present 2D PhCWG exhibits excellent optical characteristics, as shown by near-field microscopy, by illustrating good confinement of propagating light in the line defect at wavelengths in the telecommunications range with encouragingly low losses.

Acknowledgment. This research was supported by the MESA+ Institute for Nanotechnology and is part of the Strategic Research Orientations "Advanced Photonic Structures" and "Nanofabrication". This work was also partially supported by NanoNed, a nanotechnology program of the Dutch Ministry of Economic Affairs. Of the CMAL/MESA+, Mark A. Smithers is acknowledged for operating the high-resolution SEM.

Supporting Information Available: Experimental information. This material is available free of charge via the Internet at http://pubs.acs.org.

References

(1) Yablonovitch, E. *Phys. Rev. Lett.* **1987**, *58*, 2059.
(2) John, S. *Phys. Rev. Lett.* **1987**, *58*, 2486.
(3) Joannopoulos, J. D.; Villeneuve, P. R.; Fan, S. *Nature* **1997**, *386*, 143.
(4) Joannopoulos, J. D.; Meade, R. D.; Winn, J. N. *Photonic crystals—Molding the flow of light*; Princeton University Press: Princeton, NJ, 1995.
(5) Painter, O.; Lee, R. K.; Scherer, A.; Yariv, A.; O'Brien, J. D.; Dapkus, Kim, I. *Science* **1999**, *284*, 1819.
(6) Krauss, T. F.; De la Rue, R. M.; Brand, S. *Nature* **1996**, *383*, 699.
(7) Notomi, M.; Shinya, A.; Yamada, K.; Takahashi, J.; Takahashi, C.; Yokohama, I. *IEEE J. Quantum Electron.* **2002**, *38*, 736.
(8) Bogaerts, W.; Baets, R.; Dumon, P.; Wiaux, V.; Beckx, S.; Taillaert, D.; Luyssaert, B.; Van Campenhout, J.; Bienstman, P.; Van Thourhout, D. *J. Lightwave Technol.* **2005**, *23*, 401.
(9) SOI is also a suitable template for potential telecommunication applications owing to its spectral properties in the 1.5 mm wavelength range.
(10) Chou, S. Y.; Krauss, P. R.; Renstrom, P. J. *Science* **1996**, *272*, 85.
(11) (a) Schift, H.; Park, S.; Jung, B.; Choi, C.-G.; Kee, C.-S.; Han, S.-P.; Yoon, K.-B.; Gobrecht, J. *Nanotechnology* **2005**, *16*, S261. (b) Choi, C.-G.; Kee, C.-S.; Schift, H. *Curr. Appl. Phys.* **2006**, *6S1*, e8.
(12) (a) Belotti, M.; Torres, J.; Roy, E.; Pépin, A.; Gerace, D.; Andreani, L. C.; Galli, M.; Chen, Y. *Microelectron. Eng.* **2006**, *83*, 1773. (b) Belotti, M.; Torres, J.; Roy, E.; Pépin, A.; Gerace, D.; Andreani, L. C.; Galli, M.; Chen, Y. *J. Appl. Phys.* **2006**, *99*, 024309. (c) Belotti, M.; Galli, M.; Bajoni, D.; Andreani, L. C.; Guizzetti, G.; Decanini, D.; Chen, Y. *Microelectron. Eng.* **2004**, *73—74*, 405.
(13) Borel, P. I.; Bilenberg, B.; Frandsen, L. H.; Nielsen, T.; Fage-Pedersen, J.; Lavrinenko, A. V.; Jensen, J. S.; Sigmund, O.; Kristensen, A. *Opt. Express* **2007**, *15*, 1261.
(14) (a) Faircloth, B.; Rohrs, H.; Tiberio, R.; Ruoff, R.; Krchnavek, R. R. *J. Vac. Sci. Technol. B* **2000**, *18*, 1866. (b) Carlberg, P.; Graczyk, M.; Sarwe, E.-L.; Maximov, I.; Beck, M.; Montelius, L. *Microelectron.*

Eng. **2003**, *67*−*68*, 203. (c) Nakamatsu, K.; Watanabe, K.; Tone, K.; Katase, T.; Hattori, W.; Ochiai, Y.; Matsuo, T.; Sasago, M.; Namatsu, H.; Komuro, M.; Matsui, S. *Jpn. J. Appl. Phys* **2004**, *43*, 4050.
(15) (a) Lebib, A.; Chen, Y.; Carcenac, F.; Cambril, E.; Manin, L.; Couraud, L.; Launois, H. *Microelectron. Eng.* **2000**, *53*, 175. (b) Kim, S. H.; Hiroshima, H.; Inoue, S.; Kurashimma, Y.; Komuro, M. *J. Vac. Sci. Technol. B* **2003**, *21*, 3144. (c) Shi, J.; Peroz, C.; Peyrade, D.; Salari, J.; Belotti, M.; Huang, W. H.; Chen, Y. *Microelectron. Eng.* **2006**, *83*, 1664.
(16) Kooi, E. *The Invention of LOCOS - IEEE Case Histories of Achievement in Science and Technology*; IEEE: New York, 1991; Vol. 1, pp 101−128.
(17) Baba, T.; Motegi, A.; Awai, T.; Fukaya, N.; Watanabe, Y.; Sakai, A. *IEEE J. Quantum Electron.* **2002**, *38*, 743.
(18) Haneveld, J.; Jansen, H.; Berenschot, E.; Tas, N.; Elwenspoek, M. *J. Micromech. Microeng.* **2003**, *13*, S62.
(19) At room temperature, a silicon etch rate in the <110> direction, i.e., the direction perpendicular to the wafer surface of the <110> silicon wafer, of 3.7 nm•min^{-1} was found along with an excellent etch uniformity (± 1 nm) over the entire 4-in. wafer and a selectivity of (at least) 250 with respect to SiO_2 as the etch mask.
(20) Notomi, M.; Shinya, A.; Yamada, K.; Takahashi, J.; Takahashi, C.; Yokohama, I. *Electron. Lett.* **2001**, *37*, 293.
(21) Yamada, K.; Notomi, M.; Shinya, A.; Takahashi, C.; Takahashi, J.; Morita, H. *Electron Lett.* **2002**, *38*, 74.
(22) Feature dimension analysis of the diameter (*d*) and periodicity (*a*) was done by statistical calculation of about 20 measurements from the high-resolution SEM images. Each feature was fit by a circle in order to determine the feature diameter. The periodicity was taken as the distance of the centers from two adjoining features.
(23) The deviation between the design diameter and the actual diameter therefore is a result of the accuracy of the milling process. The cause of the deviation could reside in the current beam overlap of the milling process and the feature definition in the stream file. At exporting the vector design in CorelDraw12 into a 240 dpi tiff file, the program approximates the circular elements into an integer number of dots. At 240 dpi (i.e., 94 dots per cm), the diameter of each element consists of 19−20 dots. Theoretically, the resulting diameter of the circular elements after translation into a stream file is in the range of 218−230 nm (number of dots × DAC value). See the Supporting Information for further details.
(24) Lim, H.; Lee, Y.; Han, S.; Cho, J.; Kim, K.-J. *J. Vac. Sci. Technol. A* **2001**, *19*, 1490.
(25) Jansen, H. V.; De Boer, M. J.; Wiegerink, R.; Tas, N.; Smulders, E.; Neagu, C.; Elwenspoek, M. *Microelectron. Eng.* **1997**, *35*, 45.
(26) Austin, M. D.; Ge, H.; Wu, W.; Li, M.; Yu, Z.; Wasserman, D.; Lyon, S. A.; Chou, S. Y. *Appl. Phys. Lett.* **2004**, *84*, 5299.
(27) (a) Gersen, H.; Karle, T. J.; Engelen, R. J. P.; Bogaerts, W.; Korterik, J. P.; Van Hulst, N. F.; Krauss, T. F.; Kuipers, L. *Phys. Rev. Lett.* **2005**, *94*, 073903. (b) Gersen, H.; Karle, T. J.; Engelen, R. J. P.; Bogaerts, W.; Korterik, J. P.; Van Hulst, N. F.; Krauss, T. F.; Kuipers, L. *Phys. Rev. Lett.* **2005**, *94*, 123901.
(28) For a topical review on near-field characterization of PhCWGs: Bozhevolnyi, S. I.; Kuipers, L. *Semicond. Sci. Technol.* **2006**, *21*, R1.
(29) Volkov, V. S.; Bozhevolnyi, S. I.; Frandsen, L. H.; Kristensen, M. *Nano Lett.* **2007**, *7*, 2341.
(30) Peeters, C.; Flück, E.; Balistreri, M. L. M.; Otter, A. M.; Kuipers, L.; Van Hulst, N. F. *Appl. Phys. Lett.* **2000**, *77*, 142.
(31) This is a characteristic feature of Bloch modes−general wave functions with a periodic amplitude modulation that coincides with the periodic modulation of the potential (in this case, the dielectric constant). See: Kittel, C. *Introduction to Solid State Physics*, 8th ed.; Wiley: New York, 2005.
(32) Balistreri, M. L. M.; Klunder, D. J. W.; Blom, F. C.; Driessen, A.; Hoekstra, H. J. W. M.; Korterik, J. P.; Kuipers, L.; Van Hulst, N. F. *Opt. Lett.* **1999**, *24*, 1829.
(33) Engelen, R. J. P.; Karle, T. J.; Gersen, H.; Korterik, J. P.; Krauss, T. F.; Kuipers, L.; Van Hulst, N. F. *Opt. Express* **2005**, *13*, 4457.
(34) Engelen, R. J. P.; Sugimoto, Y.; Gersen, H.; Ikeda, N.; Asakawa, K.; Kuipers, L. *Nat. Phys.* **2007**, *3*, 401.
(35) The propagation losses for light of TE polarization were determined at different excitation wavelengths from a linear fit of the intensity profiles assuming that the interaction between the probe and the waveguide remains constant over the entire scan area.
(36) Tanaka, Y.; Asano, T.; Hatsuta, R.; Noda, S. *J. Lightwave Technol.* **2004**, *22*, 2787.

NL801615C